High-Performance Sono-Piezoelectric Nanocomposites Enhanced by Interfacial Coupling Effects for the Implantable Nanogenerators and Actuators

Yingxin Chen[1#,], Jingchao Shi[1#], Guowei Yang[4#], Ning Zhu[1], Lei Zhang[2], Dexin Yang[1], Ni Yao[3], Wentao Zhang[5], Yongshuang Li[1], Qiyun Guo[4], Yuxiang Wang[4], Yan Wang[4], Tao Yang[1], Xiaolian Liu[1], Jian Zhang[1*]*

1. International Research Center for EM Metamaterials and Institute of Advanced Magnetic Materials, Hangzhou Dianzi University, Hangzhou, 310018, China.
2. State Key Laboratory of Electrical Insulation and Power Equipment, Xi'an Jiaotong University Xi'an, 710049, China.
3. Research Center for Intelligent Sensing, Zhejiang Lab, Hangzhou, 311121, China.
4. School of Communication Engineering, Hangzhou Dianzi University, Hangzhou, 310018, China. Corresponding author email: yxchen@hdu.edu.cn; jianzhang@hdu.edu.cn
5. College of Pharmaceutical Sciences, Zhejiang University, Hangzhou, 310058, China.

Experimental Materials. The piezoelectric matrix P(VDF-CTFE) (mole ratio, 91:9) was purchased from Solvay. The high-piezoelectric nanofillers (Barium titanate nanoparticles $BaTiO_3$, BT) were purchased from sigma-Aldrich. The diameter of BT NPs was approximately 50 nm. The glucose were purchased from Maklin Inc..

Synthesis of the core-shell structured BT@Carbon NPs. In the hydrothermal reaction process, 1.0 g BT NPs was dispersed in to 10 mL glycerin by ultrasound to form a suspension. Then, a different amount of glucose with 0.2 g and 0.4 g was firstly added in 40 ml water, and then mixed into the suspension, which was used to control the thickness of carbon shell. The mixture was sealed in a 100 mL Teflon-lined stainless-steel autoclave, and placed in the vacuum oven at 170 ℃ for 4 hours. Then, the reactor was cooled to room temperature. The as-prepared nanoparticles were purified with distilled water for three times and collected by centrifugation. In the carbonization process, the BT@Glucose NPs were carbonized by heat treatment in a tube furnace with Ar-shield at 500 °C for 3 hours. Finally, two thickness of carbon shell were successfully synthesized onto the surface of BT

NPs, which was named as 3.9 nm BT@Carbon NPs and 8.9 nm BT@Carbon NPs according to TEM images.

Preparation of P(VDF-CTFE)/BT@Carbon Nanocomposites. A different amount of 8.9 nm BT@Carbon NPs with 0.012, 0.028, 0.04 and 0.06 g were firstly dispersed in the *N, N*-dimethylformamide (DMF, 5ml) solution by ultrasound for 30 min to form a suspension. Then, 0.4 g P(VDF-CTFE) matrix was added into the suspension to obtain 3%, 6%, and 9% P(VDF-CTFE)/ 8.9 nm BT@Carbon nanocomposites. The mixtures were placed on the telflon plates to form the films in the oven for 48 h. Then, the films were treated in the vacuum oven for 24 h to remove residual DMF solvent. Finally, 30 mg nanocomposite films were placed in the mold and hot-pressed at 180 ^{o}C and 5 MPa for 3 min. The thickness of the obtained film is about 20~30 μm for the electric tests. In the same preparation process, we also prepared 9% P(VDF-CTFE)/ 3.9 nm BT@Carbon nanocomposites, and 9% P(VDF-CTFE)/ 3.9 nm BT@Carbon nanocomposites for comparison.

Characterization.

TEM mapping. The morphology of BT@Carbon NPs and elemental mapping were carried out by transmission electron microscopy (TEM, ThermoFisher Talos F200S).

SEM mapping. The cross-section feature of the nanocomposites with BT NPs and BT@Carbon NPs were obtained by scanning electron microscopy (SEM, JEOL JSM6460-LV) and energy-dispersive spectroscopy (EDS) at 15 kV. The cross-section of the samples was prepared by cutting off the samples in the liquid nitrogen. A gold layer of 10 μm was sprayed onto the cross-section of the samples to avoid accumulation of charges.

TGA analysis. The grafting degree of the carbon shell of BT@Carbon NPs were investigated using Thermogravimetric analysis (SDTA 851, Mettler Toledo) at the air atmosphere. The thermal

program used for testing is a heating rate of 20 °C min^{-1}, a temperature range from 25 °C to 900 °C, a total weigh of 7-10 mg. The samples were placed in ceramic crucibles.

Raman spectra. All the Raman spectra of BT@Carbon nanoparticles were measured on a LabRAM (Horiba) Raman spectrometer in air at room temperature. The excited wavenumber of the laser is 514 nm (2.41 V).

Flash DSC measurements. The interfacial crystallization of the nanocomposites was performed by using the apparatus of flash differential scanning calorimetry (Flash DSC1, Mettler-Toledo Co.) with mechanical-intercooler (TC 100MT, Huber) and nitrogen purge gas. The chip-sensor of MultiSTAR UFS1 (XI-400, Xensor Integrations, NL) was conditioned five times and corrected one time according to the standard procedure prior to use at the heating and cooling rate of 1000 $K.s^{-1}$. The sample was cut into the testing specimens of 60~100 ng under the help of a scalpel and microscope. The specimens were placed onto the testing area of the center sensor by a feather. Finally, Flash DSC 1 executed the experiment programs to achieve the heat flow rates used to calculate the heat capacity and enthalpy changes on fast heating.

Water contact angle. Water contact angles of the nanoparticles were performed using the contact angle goniometer (DSA25, KRÜSS) at the relative humidity of 50% and room temperature. The nanoparticles were dispersed in the water, deposited onto the silicon substrate, and dried in a vacuum oven for 24h. Then, each droplet of 2 μL was placed onto the silicon substrate to measure water contact angle. Each sample was tested at least five times.

Dielectric properties. The dielectric constant and loss as a function of the frequency range from 100 Hz to 10^6 Hz were performed via a high-precision LCR meter (HP4284A, Agilent).

Ferroelectric properties. Ferroelectric P-E hysteresis loops were measured by using an artificial intelligence ferroelectric system (Poly K).

Resistance. The resistance of PENGs dependence on time was collected by CH Instruments (model, CHI800D) and a computer installed with CHI800D software.

Output performance of PENGs. First, the nanocomposite membranes were implanted at different depths of the porcine tissue. Second, the output voltages and current, which was generated on the membranes under ultrasound stimulation with continuous and pulse waves different power (i.e., 15 W, 45 W, 75 W, 105 W, and 135 W), were collected using an oscilloscope (Rigol, DS1102E) and a programmable electrometer (6514, Keithley Instruments model), respectively.

Cell biocompatibility. The biocompatibility was determined by CCK-8 assay (BEIJING LABLEAD BIOTECH CO.,LTD.) as the manufacturer instructed. Briefly, $1*10^5$ B-16 cells and 3 mg of each material was placed in 96-well plate and incubated for 24 h. Fluorescence image was obtained by DAPI staining of B16 24 h after co-incubation.

Animal experiments. All studies were conducted according to ethical regulations and protocols approved by the Institutional Animal Care and Use Committee (ZJCLA, NO. ZJCLA-IACUC-20010320). The SD mice (6 to 8 weeks of age) were purchased from Hangzhou Medical College. The pentobarbital sodium with 1% was injected into the abdominal cavity of the mice. After anesthesia, the back hairs were shaved, and the skin was cut open by an operating knife. The P(VDF-CTFE) and P(VDF-CTFE)/BT@Carbon nanocomposite membranes were implanted into the back for biocompatibility testing and output performance. After the treatment of 14 days, the blood samples of the control and the experimental groups were collected to test biomedical indexes. The structure of mice organs (heart, lung, liver, kidney, and the skin) were also collected for comparison.

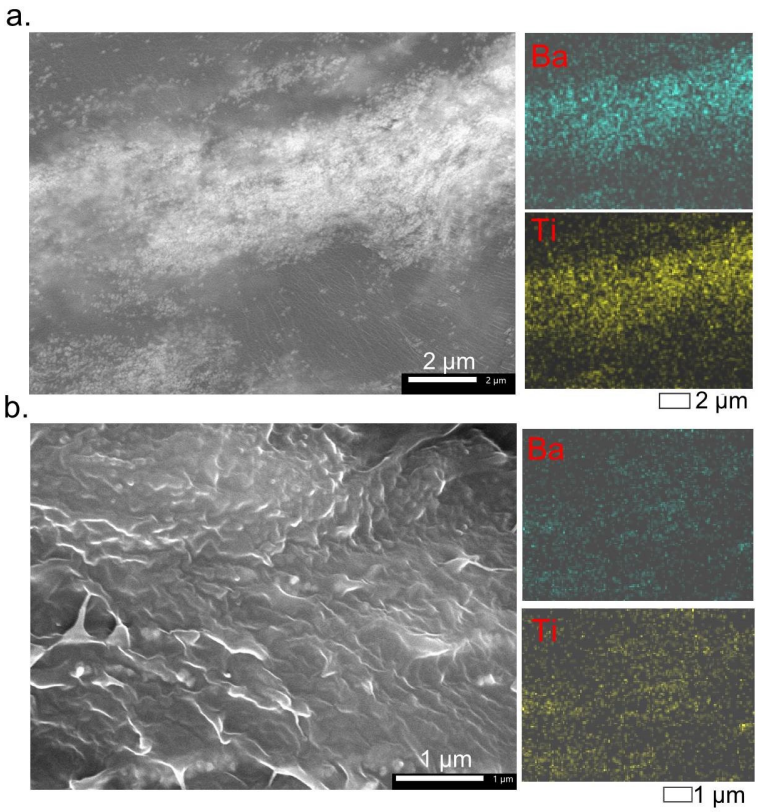

Figure S1. Distribution of BT@Carbon NPs. SEM photos and EDS element mapping of (a) 9% P(VDF-CTFE)/BT and (b) 9% P(VDF-CTFE)/BT@Carbon nanocomposites.

Dispersion of BT@Carbon NPs. Cross-sectional morphologies of P(VDF-CTFE)-based nanocomposites with 9 wt% BT and 9 wt% BT@Carbon NPs are shown in Figure S1a and S1b. As expected, unmodified BT NPs were not well-separated at high content of 9% BT NPs. EDS was employed to demonstrate the existence of BT fillers in the P(VDF-CTFE) matrix, as clearly illustrated in Figure S1a. The brighter zone in the element color mapping of Ba and Ti atoms indicates a series nanoparticle aggregation of $BaTiO_3$ NPs in the P(VDF-CTFE) matrix. After surface-modified $BaTiO_3$@Carbon NPs, Ba and Ti atoms, which come from the $BaTiO_3$@Carbon NPs, are uniformly dispersed in the P(VDF-CTFE) matrix at the same concentrations of 9% due to

the enhanced interfacial adhesion between BT@Carbon NPs and P(VDF-CTFE) matrix, as shown in Figure S1.

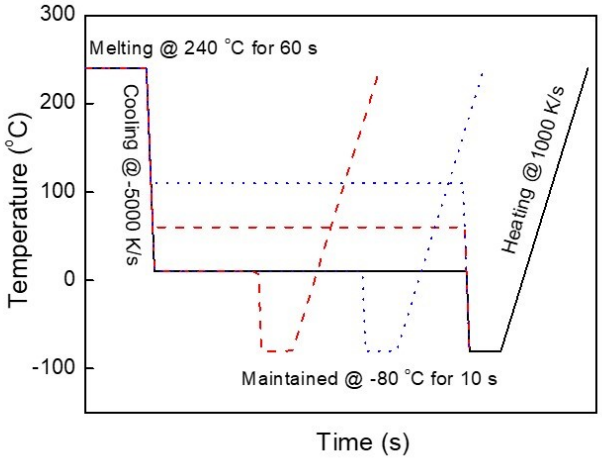

Figure S2. Time-temperature programs of PVDF-based nanocomposites annealed at the various time and temperature for crystallization, followed with heating scans at constant heating rate of 1000 K/s. The speed of each rapid cooling process is 5000 K/s to avoid crystallization in advance.

We started with the observation on the time evolution of low crystallization of PVDF-based nanocomposites at low-temperature region between the glass transition and melting temperature to compare crystallization halftimes between P(VDF-CTFE) and PVDF-based nanocomposites. The temperature programs of isothermal crystallization are depicted in Fig. S3. First, the samples were kept at the melting temperature of 240 °C for 10 s to erase the thermal history. Second, the samples were cooled down to the specific crystallization temperature for isothermal crystallization at various periods and at various low temperatures ranging from -10 to 120 °C. Third, the samples were cooled down to -80 °C at the rate of 5000 K/s for 5 min. Finally, they were heated from -80 °C to 240 °C at the heating rate of 1000 K/s.

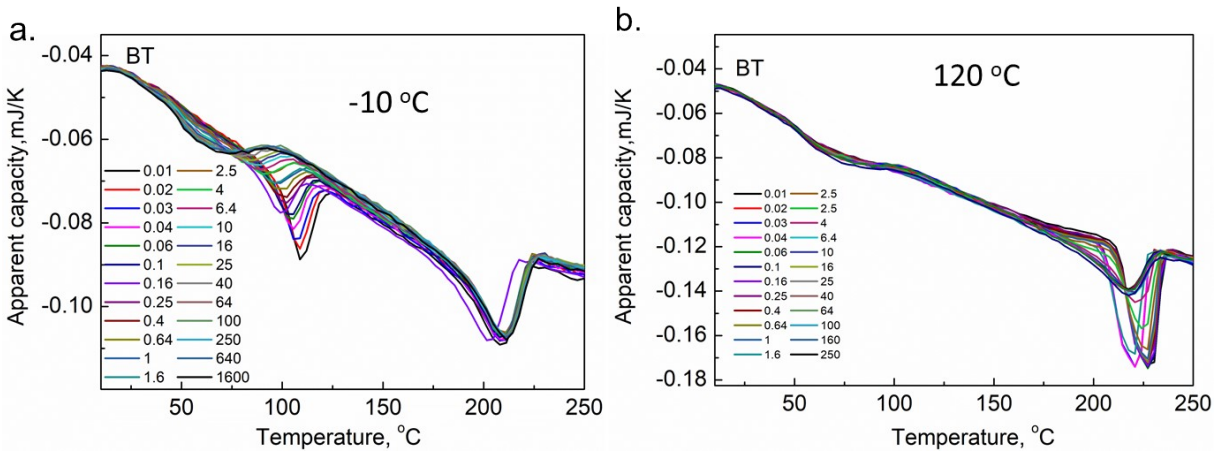

Figure S3. Heating curves of heat capacities of 9% P(VDF-CTFE)/BT Carbon after annealed at various time durations in (a) the low temperature T_x=-10 °C, and (b) the high temperature T_x=120 °C.

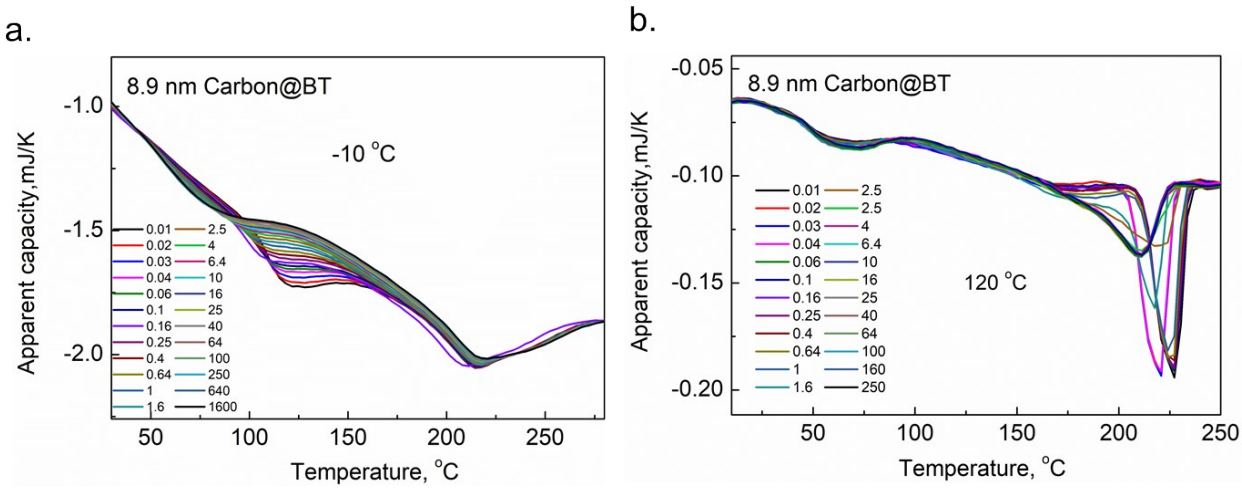

Figure S4. Heating curves of heat capacities of 9% P(VDF-CTFE)/BT@8.9 nm Carbon after annealed at various time durations in (a) the low temperature T_x=-10 °C, and (b) the high temperature T_x=120 °C.

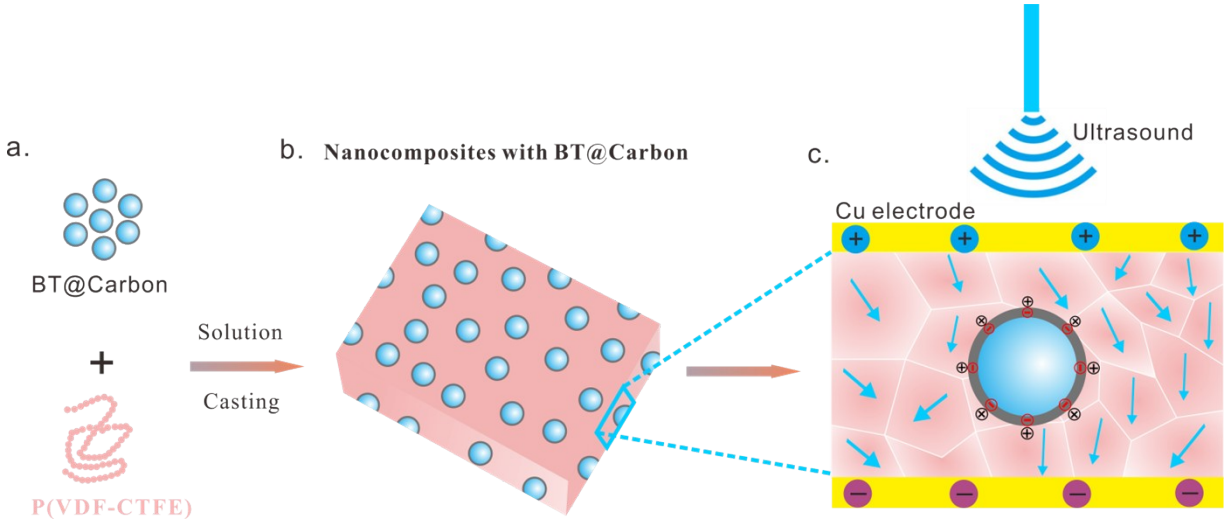

Figure S5 (a) Schematic image of BT@Carbon NPs and molecular chains of P(VDF-CTFE), the illustration of the preparation process for the fabrication of (b) the nanocomposite, and (c) ultrasound-activated piezoelectric nanocomposites.

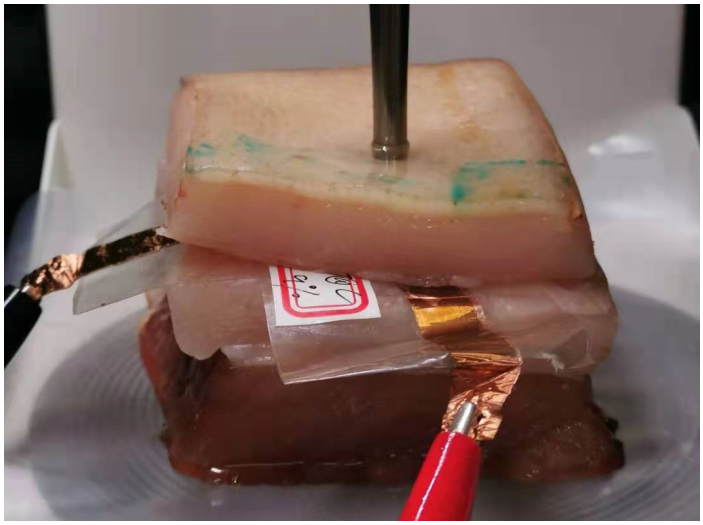

Figure S6. Digital photo showing piezoelectric nanogenerations (PENGs) implanted into the streaky pork under US stimulation.

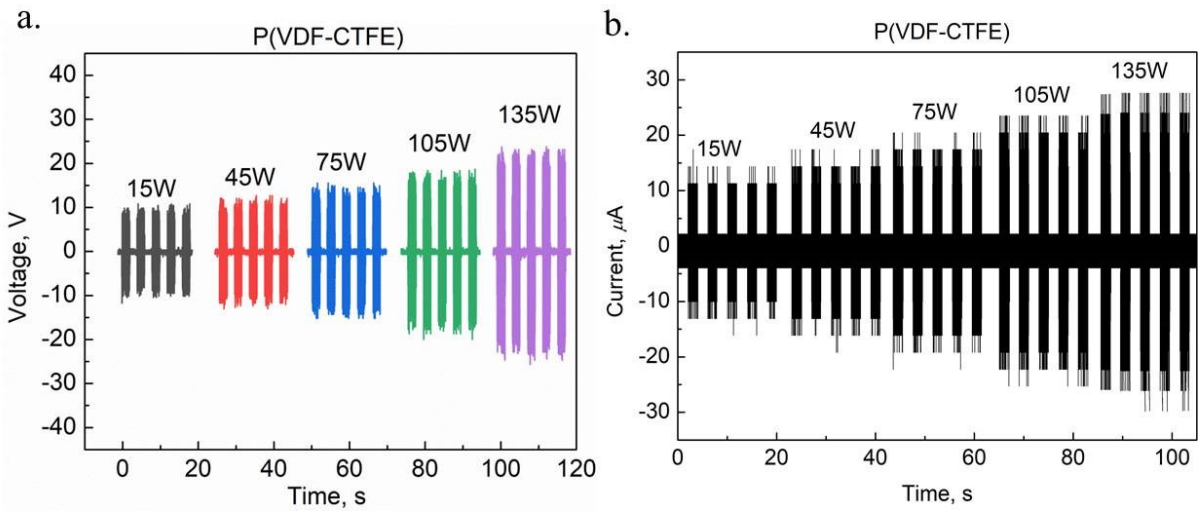

Figure S7. (a) The voltage with a load of 100 kΩ, (b) the short-circuit current of P(VDF-CTFE) under a series of ultrasonic power of 15, 45, 75, 105 and 135 W.

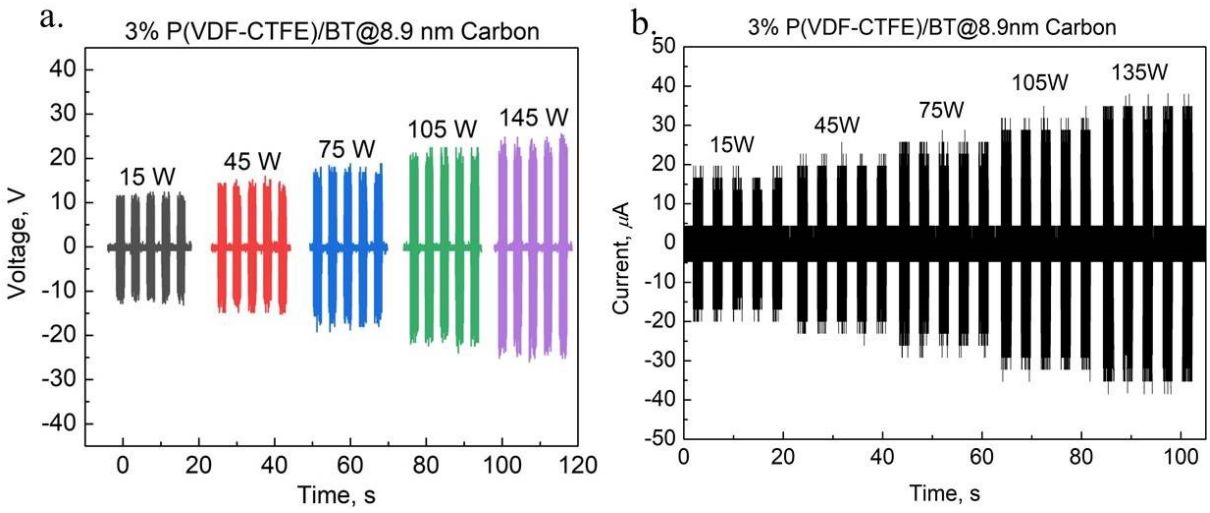

Figure S8. (a) The voltage with a load of 100 kΩ, (b) the short-circuit current of the nanocomposites with 3% BT@8.9 nm Carbon under a series of ultrasonic power of 15, 45, 75, 105 and 135 W.

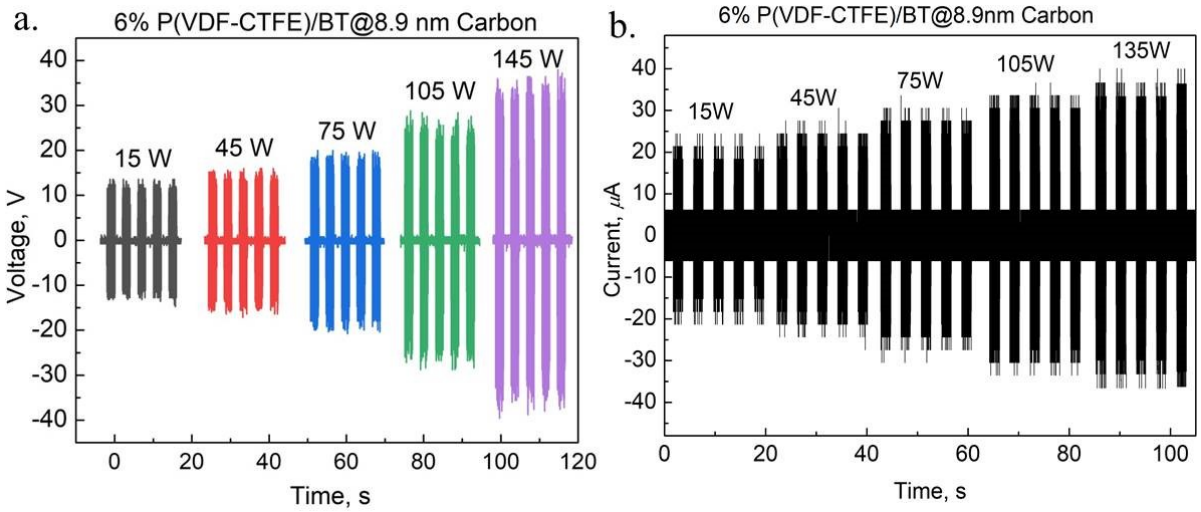

Figure S9. (a) The voltage with a load of 100 kΩ, (b) the short-circuit current of the nanocomposites with 6% BT@8.9 nm Carbon under a series of ultrasonic power of 15, 45, 75, 105 and 135 W.

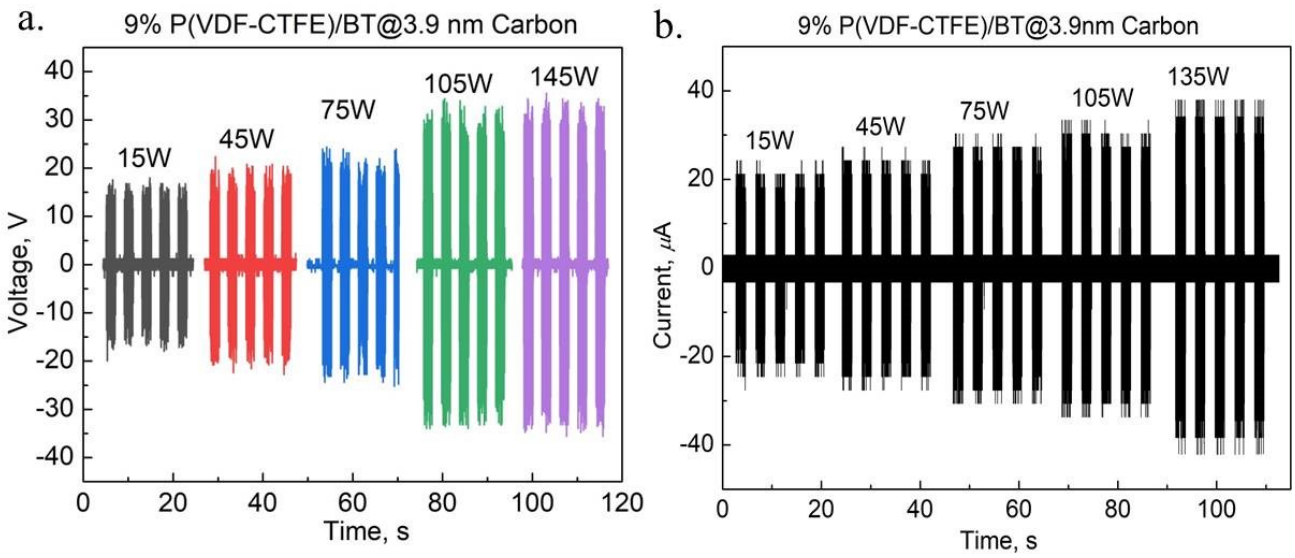

Figure S10. (a) The voltage with a load of 100 kΩ, (b) the short-circuit current of the nanocomposites with 9% BT@3.9 nm Carbon under a series of ultrasonic power of 15, 45, 75, 105 and 135 W.

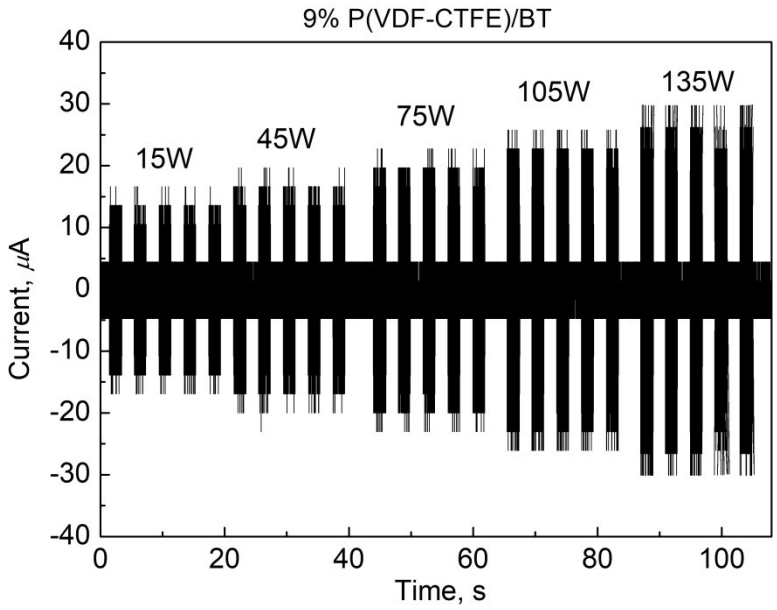

Figure S11. The voltage with a load of 100 kΩ of 9% P(VDF-CTFE)/BT nanocomposites under a series of ultrasonic power of 15, 45, 75, 105 and 135 W.

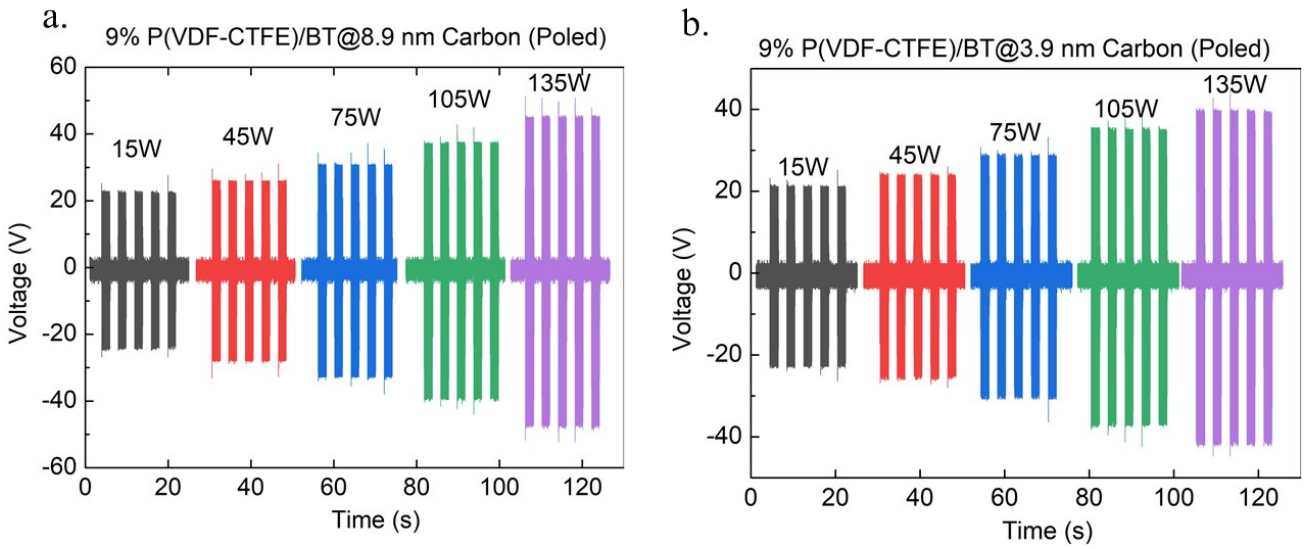

Figure S12. The voltage with a load of 100 kΩ of the poled nanocomposites with (a) 9% BT@3.9 nm Carbon, (b) 9% BT@8.9 nm Carbon under a series of ultrasonic power of 15, 45, 75, 105 and 135 W.

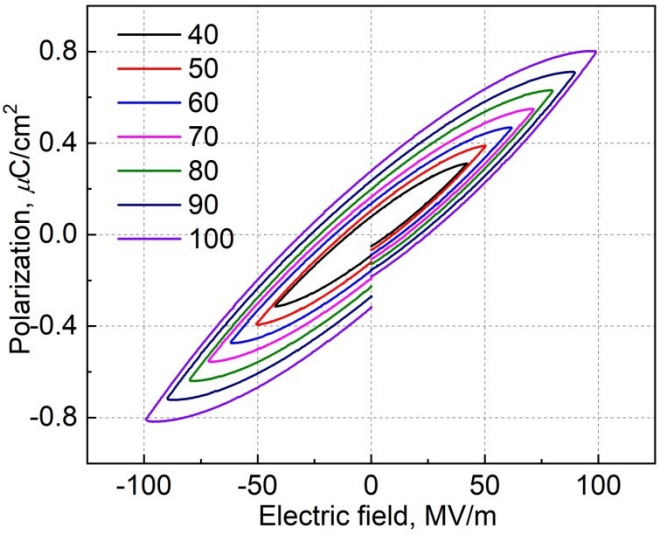

Figure S13. Bipolar P-E hysteresis loops of the unpoled P(VDF-CTFE).

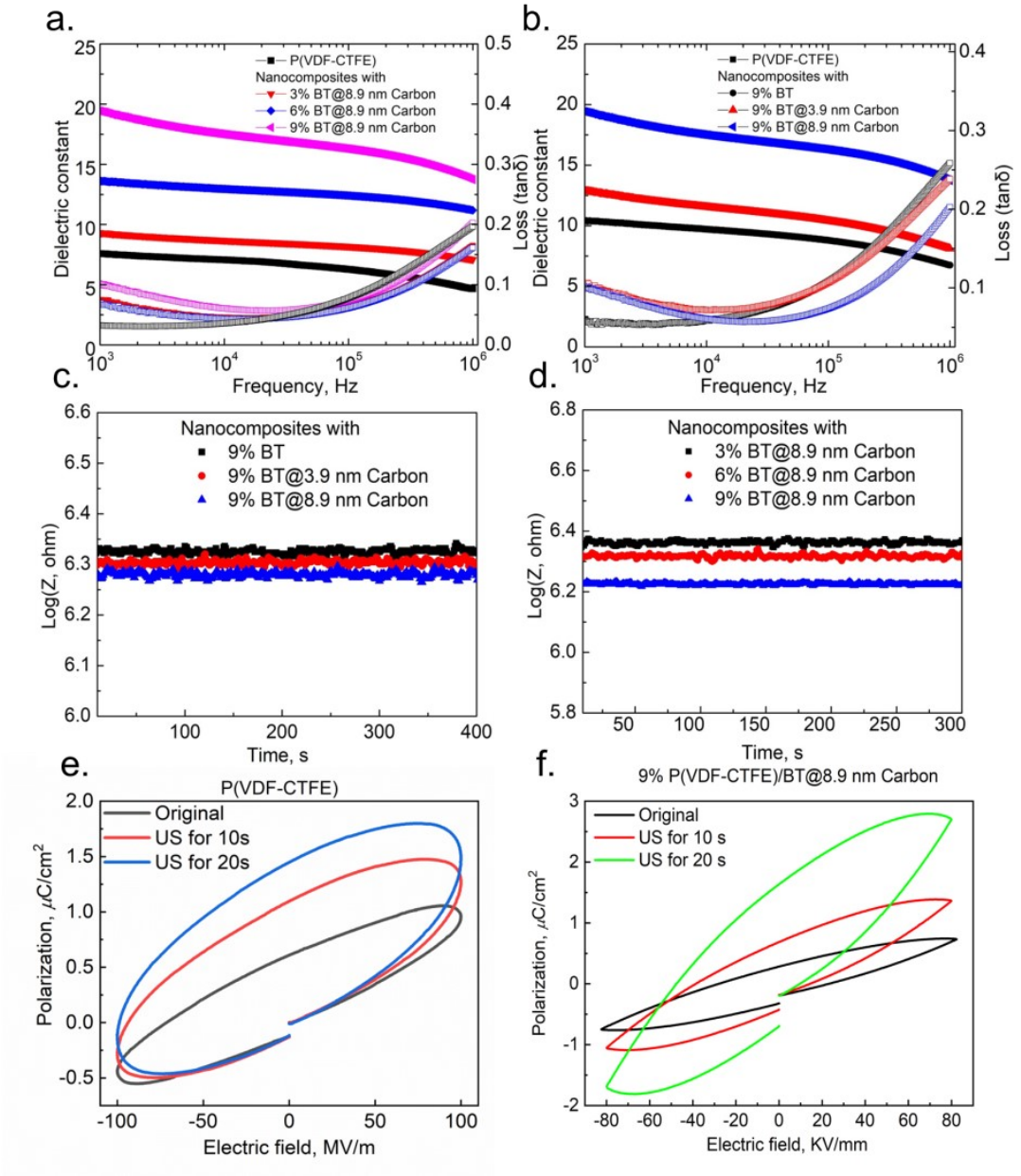

Figure S14. Dielectric constant and loss of the nanocomposites with (a) various mass content of BT@Carbon NPs, (b) and different thickness of carbon shell measured from 10^3 Hz to 1 MH. (c) Electrical resistivity of nanocomposites of (c) various mass content of BT@Carbon NPs, (d) and different thickness of carbon shell. Bipolar P-E hysteresis loops of (e) P(VDF-CTFE) at the field of 100 MV/m, and (f) 9% P(VDF-CTFE)/BT@9 nm Carbon nanocomposites at the field of 80 MV/m after US stimulation for 0, 10 s and 20 s.

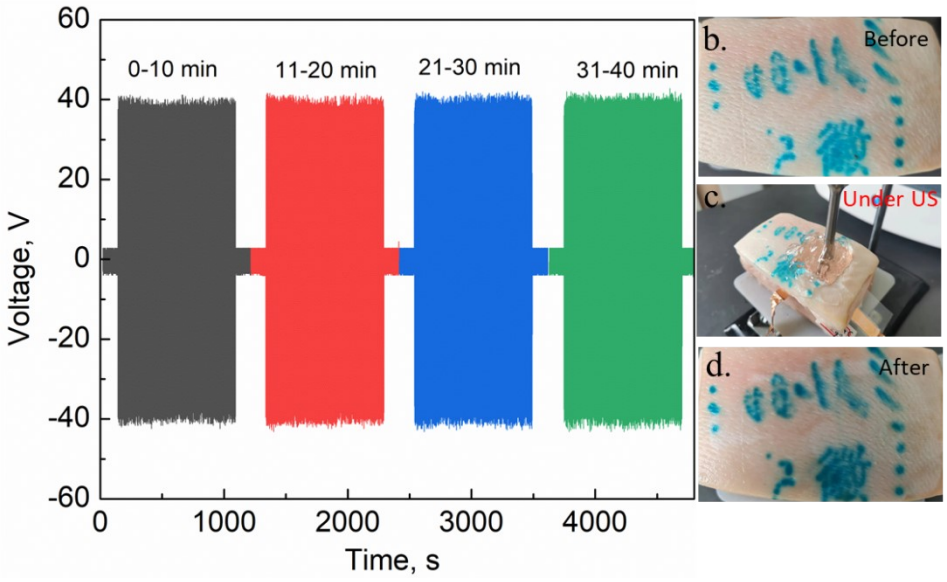

Figure S15. (a) Long-term durability test of 9% P(VDF-CTFE)/BT@Carbon nanocomposite for 40 min at the ultrasonic power of 75 W. The pictures showing the state of the pork (b) before, (c) under, (d) after US stimulation for 40 min.

For long-term durability test, the copper tape with a dimension of 3 cm×3 cm was placed onto the pork tissue. The output voltage of the 9% P(VDF-CTFE)/BT@8.9 nm Carbon membrane kept constant at the ultrasonic power of 75 W for 40 min, and its voltage was about 40 V. Before and after US stimulation, the state of the pork tissue seems intact, as shown in Figure S14. Under the pressure of US with sinusoidal waveform, the dipoles vibrate and move up and down, generating an AC electric output with positive and negative potential corresponding to the peaks and troughs of ultrasonic wave, as shown in Figure S15.

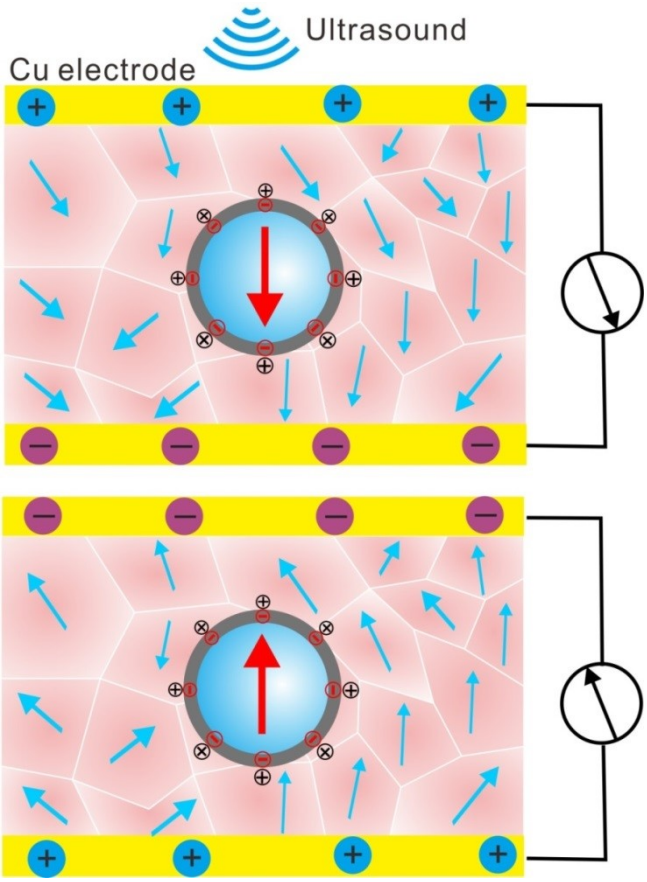

Figure S16. The mechanism of ultrasound-activated piezoelectric nanogenerators.

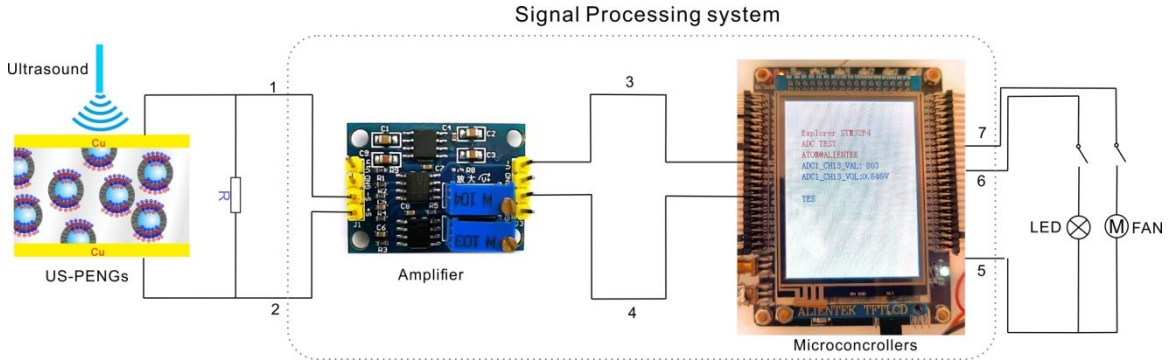

Figure S17. Circuit diagram of US-driven peizoelectric actuators.

Table S1. Body weight changes in the mouse for 0, 4, 8, 12, and 14 days after the implantation of the P(VDF-CTFE)/BT@Carbon nanocomposite group and the control group.

Group	0 Day		4 Days		8 Days		12 Days		14 Days	
P(VDF-CTFE)/BT@Carbon	1	20.3	1	18.6	1	20.4	1	20.8	1	21.7
	2	22.2	2	22.4	2	23.5	2	23.9	2	25.1
	3	22	3	22.2	3	22.9	3	22.4	3	23.5
	4	23.2	4	22.9	4	23.6	4	24.2	4	25.2
	21.925±1.203		21.525±1.972		22.600±1.500		22.825±1.563		23.875±1.646	
Control	1	22.8	1	22.2	1	23.4	1	23.5	1	22.5
	2	21.3	2	21.9	2	22	2	22.5	2	24.3
	3	21.6	3	22.4	3	22.8	3	23.2	3	25.4
	4	21	4	21.5	4	21.8	4	21.9	4	22.7
	21.675±0.789		22.012±0.392		22.500±0.739		22.775±0.718		23.725±1.377	

Table S2.Functional indexes of liver and kidney of the mouse for 14 days after the implantation of the P(VDF-CTFE)/BT@Carbon nanocomposite group and the control group.

Group	ALT		CRE-J		AST		UREA	
P(VDF-CTFE)/BT@Carbon	1	36.4	1	35.4	1	89.1	1	9.73
	2	60.7	2	35.4	2	91.9	2	12.05
	3	39.1	3	35.4	3	94.3	3	9.94
	4	38.8	4	36.8	4	96	4	11.44
	43.75±11.364		35.750±0.700		92.825±3.000		10.790±1.133	
Control	1	36.4	1	37.5	1	131.1	1	8.43
	2	55.9	2	34	2	118.4	2	10.54
	3	37.7	3	36.8	3	71.9	3	13.19
	4	66.2	4	36.1	4	121.1	4	10.24
	49.05±14.490		36.100±1.512		110.625±26.388		10.600±1.962	

Table S3. The indexes of the blood samples of the mouse for 14 days after the implantation of the P(VDF-CTFE)/BT@Carbon nanocomposite group and the control group.

Group	WBC (10^9/L)		RBC (10^12/L)		HGB (g/L)		PLT (10^9/L)	
P(VDF-CTFE)/BT@Carbon	1	7.48	1	9.02	1	170	1	1428
	2	10.24	2	9.14	2	166	2	1475
	3	10.82	3	9.11	3	166	3	1577
	4	10.78	4	9.39	4	172	4	1334
	9.830±1.589		9.165±0.158		168.502±3.010		1453.500±101.069	
Control	1	9.42	1	8.95	1	166	1	1132
	2	7.11	2	8.88	2	166	2	1355
	3	11.4	3	8.74	3	163	3	1315
	4	8.45	4	9.3	4	178	4	1272
	9.095±1.805		8.968±0.239		168.251±6.652		1268.521±97.106	